Crystal structure, magnetic properties, and Mössbauer studies of $La_{0.6}Sr_{0.4}FeO_{3-\delta}$ prepared by quenching in different atmospheres

J. B. Yang, W. B. Yelon, and W. J. James
Graduate Center for Materials Research and Departments of Chemistry, University of Missouri-Rolla, Rolla, Missouri 65409

Z. Chu and M. Kornecki
Department of Physics, University of Missouri-Columbia, Columbia, Missouri 65211

Y. X. Xie, X. D. Zhou, and H. U. Anderson
Center for Electronic Materials Research, University of Missouri-Rolla, Rolla, Missouri 65409

Amish G. Joshi and S. K. Malik
Tata Institute of Fundamental Research, Colaba, Mumbai 400-005, India

(Received 20 December 2001; revised manuscript received 28 August 2002; published 13 November 2002)

Samples of $La_{0.6}Sr_{0.4}FeO_{3-\delta}$ compounds prepared by quenching in different gaseous environments were studied by x-ray diffraction, neutron diffraction, magnetization measurements, and Mössbauer spectroscopy (MS). All materials are single phase and crystallize in the rhombohedral perovskite structure. Samples prepared in flowing air, N_2, and O_2 yielded oxygen vacancies ranging from 0% to 1%. The oxygen vacancy concentration increases from 6.8% to 9.6% as the ratio of CO/CO_2 changes from 10:90 to 90:10. The air-, N_2-, and O_2-quenched samples have a magnetic ordering temperature in the range of 300–325 K. The magnetic ordering temperature increases for all the samples subjected to the reducing CO/CO_2 atmosphere. The neutron data refinements and magnetization data indicate that the Fe sublattice of $La_{0.6}Sr_{0.4}FeO_{3-\delta}$ has an antiferromagnetic structure below the magnetic ordering temperature. The Fe atoms possess a magnetic moment of $3.8\mu_B$ and a hyperfine field of 53 T in the CO/CO_2-quenched samples. It is found that the heat treatment in the CO/CO_2 atmosphere creates more oxygen vacancies, changes the Fe valence states, and increases the unit cell volume. In the meantime, the Fe-O-Fe bond angle increases. These dramatically affect the Fe-O-Fe superexchange coupling. The change of the Fe-O-Fe bond angle and the change of the Fe valence states in the CO/CO_2 heat treatment play a key role in the increase of the magnetic ordering temperatures and the magnetic moment. Therefore by creating oxygen vacancies or having excess oxygen, the exchange interaction of Fe-O and the valence state of Fe ions are affected, and lead to large changes in the magnetic properties, such as the magnetic ordering temperature, the magnetic moments, and the hyperfine interactions in the pervoskite structure.

DOI: 10.1103/PhysRevB.66.184415 PACS number(s): 75.50.Ee, 61.10.Nz, 76.80.+y, 81.40.−z

I. INTRODUCTION

In the last few years there has been a tremendous interest in transition metal oxides showing strong electron correlation effects and a great deal of effort is ongoing to understand their electronic states and unusual physical properties. The strong electron correlations give rise to high-temperature superconductivity in cuprate oxide systems and colossal magnetoresistance in manganites, to name a few features. Mixed valence and structural changes of these materials lead to charge ordering phenomena, diverse magnetic structures, metal insulator phase transitions, and other phenomena of fundamental and potentially technological importance.

Among the transition metal oxides, perovskite compounds of the type $R_{1-x}A_xBO_{3-\delta}$, where R is a rare earth, A is Ba, Ca, or Sr, B is Fe, Mn, Co, or Ni, are of considerable importance, due to their interesting electrical, magnetic, and catalytic properties.[1,2] In particular, the Mn and Fe compounds have been extensively studied as regards their magnetic and transport properties.[3–8] These systems are characterized by mixed-valent transition metal ions that are responsible for high electronic conductivity of these materials at or near room temperature. They may also support a large oxygen nonstoichiometry, which arises from the high diffusivity of oxygen ions, and can lead to their use as selective oxygen transport membranes.[9–12] Mixed valence of the transition metal ions can be induced in these compounds either by introducing divalent ions such as Ba, Ca, or Sr at the trivalent La site or by creating oxygen vacancies. The magnetic properties of these compounds are thought to arise from a superexchange mechanism involving $3d$ electrons of the transition metal ions and oxygen p orbitals.[13] Thus oxygen plays a very important role in magnetic ordering of these compounds. Many of the Mn-based perovskites show colossal magnetoresistance behavior (see Refs. 3–7 and those cited therein).

The $LaFeO_{3-\delta}$ and related compounds have been shown to act as good membrane materials that allow transport of oxygen ions. The compound $SrFeO_3$ is a metallic perovskite that orders antiferromagnetically at 134 K. It is cubic at room temperature and remains so down to 4.2 K.[14,15] To maintain charge balance, the Fe in this compound may be thought to be in the 4+ valence state. For the oxygen-deficient compound $SrFeO_{3-\delta}$, the Néel temperature decreases and the electric conductivity changes with increasing δ from metallic to semiconducting.[14] In contrast to $SrFeO_3$, $CaFeO_3$ orders

TABLE I. Heat treatment conditions for $La_{0.6}Sr_{0.4}FeO_{3-\delta}$.

Samples	Annealing gas	Conditions
A	N_2	Annealed at 1000 °C, 24 h, quenched to 25 °C
B	Air	Annealed at 1000 °C, 24 h, quenched to 25 °C
C	O_2	Annealed at 1000 °C, 24 h, quenched to 25 °C
D	$CO:CO_2=10:90$	Annealed at 1000 °C, 24 h, quenched to 25 °C
E	$CO:CO_2=50:50$	Annealed at 1000 °C, 24 h, quenched to 25 °C
F	$CO:CO_2=90:10$	Annealed at 1000 °C, 24 h, quenched to 25 °C

antiferromagnetically at 116 K but shows the presence of Fe in two valence states between 116 and 290 K.[16–19] In comparison with $SrFeO_3$ and $CaFeO_3$ with divalent metal ions, $LaFeO_3$ (orthorhombic structure) with trivalent La ions is a charge transfer type insulator with an energy gap of about 2 eV due to strong on-site Coulomb repulsion. The Fe ions are in the nominal trivalent state. This compound is antiferromagnetically ordered with a Néel temperature of 750 K and exhibits weak parasitic ferromagnetism due to a small canting of the Fe ion magnetic moments. Substitution of trivalent La by divalent Sr forces the Fe ions into a $4+$ state.[20–23] This weakens or even destroys the magnetic ordering. The hole doping due to Sr substitution greatly reduces the resistivity at room temperature, although the compounds remain insulating at low temperatures, at least, up to $x=0.7$. Some perovskite-type $La_{1-x}Sr_xBO_{3-\delta}$ (B=Mn, Fe, Co) compounds are strongly covalent antiferromagnetic metals while others are metallic with an enhanced Pauli paramagnetism and many are magnetic insulators.[13,24–26] $LaFeO_3$ is an antiferromagnetic insulator and has an orthorhombically distorted pervoskite structure. Upon substituting Sr^{2+} for La^{3+}, the orthorhombic structure becomes pseudocubic for $x\leqslant 0.4$ in $La_{1-x}Sr_xFeO_{3-\delta}$. As for $x>0.4$, the Fe^{4+} content decreases markedly due to oxygen loss, resulting in the actual Fe^{4+} content having a maximum of about 40% for $x=0.5$.[27] When Sr^{2+} is substituted for La^{3+}, the activation energy of the semiconducting compounds and the antiferromagnetic ordering temperature decrease systematically.[27,21] There are some characteristics of the $La_{1-x}Sr_xBO_{3-\delta}$ compounds which provide the potential for technical applications: (a) mixed valence states of the $3d$ transition metals on the B sites, which result in a high electronic conductivity, (b) large oxygen nonstoichiometry, which is related to the high diffusivity of the oxide ions, and (c) formation of a solid solution with a wide miscibility range. Thus these compounds have applications as catalysts, chemical sensors, electrodes, and solid electrolyte fuel cells. Charge ordering has been found in $La_{1/3}Sr_{2/3}FeO_3$,[28] and a structural modulation accompanying the charge ordering transition has been confirmed by electron microscopy.[29] Charge ordering is also observed in some other $R_{1/3}Sr_{2/3}FeO_3$ compounds [e.g., those with Pr (Ref. 30) and Nd (Ref. 31)]. The modification of the chemical composition on the perovskite A sites and the concentration of the oxygen vacancies are effective for controlling the crystal structure and fundamental physical properties of the perovskite-type compounds. A systematic study of the effect of the oxygen content on the structural, magnetotransport, and magnetic properties has been undertaken on the series of $LaMnO_{3+\delta}$.[32–34]

In view of the importance of oxygen and the role played by the divalent ions, it is of great interest to carry out systematic studies on the $La_{1-x}Sr_xMO_{3-\delta}$ compounds as a function of the divalent ion doping and the oxygen vacancy concentration.

In this study, we report on the structure, magnetic properties, and Mössbauer spectra of the $La_{0.6}Sr_{0.4}FeO_{3-\delta}$ compounds prepared by varying heat treatment. The dependence of the structure, magnetic properties, and hyperfine interaction on the heat treatment environments has been studied in detail. The dependence of the exchange coupling on the oxygen vacancy concentration and the structure has been investigated by analyzing the experimental data. A marked increase of the magnetic ordering temperature, magnetic moments, and hyperfine field observed for the CO/CO_2-treated samples is explained on the basis of the superexchange coupling, bond distances, and angles between the Fe-O-Fe linkage.

II. EXPERIMENTAL METHODS

The liquid-mixing method[35,36] was used to prepare $La_{0.6}Sr_{0.4}FeO_3$ fine powders. An aqueous solution of Fe nitrate was first prepared and thermogravimetrically standardized. Reagent grade lanthanum carbonate, strontium carbonate, and known ratios of nitrate solutions of Fe were then mixed to form a clear solution. Citric acid and ethylene glycol were added into the nitrate solution and heated slowly to form a polymeric precursor. The latter was heated to 250 °C to form an amorphous resin. Calcination of the pulverized resin was carried out at 800 °C for 8 h. The powders were pressed at 207 MPa to form a dense bar. The bar was sintered at 1000–1200 °C for 24 h under different environments as given in Table I, followed by quenching to room temperature. The magnetization curves of the samples were measured using a superconducting quantum interference device (SQUID) magnetometer in a field of up to 6 T from 1.5 K to 800 K. A magnetic field of 50 Oe was used for the field cooling (FC) and zero field cooling(ZFC) process. The crystal phase was identified by x-ray diffraction analysis using Cu $K\alpha$ radiation. The powder neutron diffraction experiments were performed at the University of Missouri-Columbia research reactor using neutrons of wavelength $\lambda=1.4875$ Å. The data for each sample were collected over 24 h at 290 K between 2θ angles of 5° and 105° on approxi-

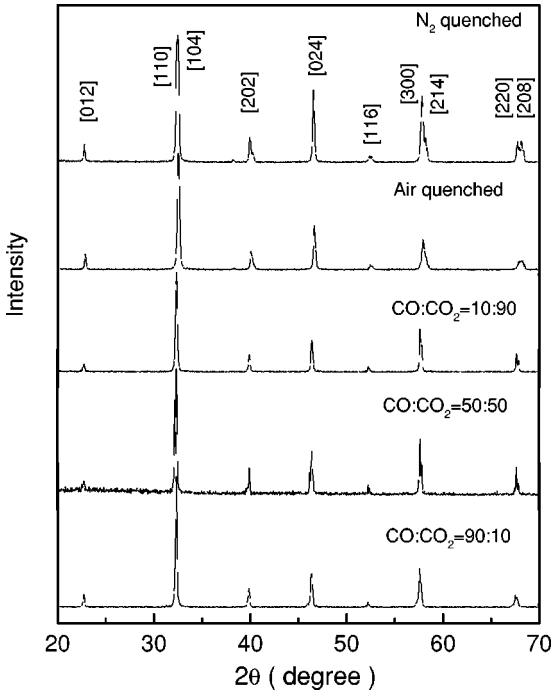

FIG. 1. Typical x-ray diffraction patterns of $La_{0.6}Sr_{0.4}FeO_{3-\delta}$ quenched in different atmospheres at room temperature.

mately 1 g of fine powders placed in a thin wall vanadium container. Refinement of the neutron diffraction data was carried out using the FULLPROF program,[37] which permits multiple phase refinement as well as magnetic structure refinements. The concentrations of the oxygen vacancies were determined by refinement of the neutron data. The Mössbauer spectra were measured using a conventional constant accelerated driver at room temperature with ^{57}Co (50 mCi) in a Rh matrix. The spectrometer was calibrated using α-Fe at room temperature and the isomer shift (IS) relative to α-Fe at 300 K.

III. RESULTS AND DISCUSSIONS

A. Crystallographic structure

Figure 1 shows the typical x-ray diffraction (XRD) patterns of $La_{0.6}Sr_{0.4}FeO_{3-\delta}$ powders at different heat treatment conditions. Similar patterns are observed for all samples, showing them to be single phase. The symmetry of the samples remains rhombohedral (space group $R\bar{3}c$) throughout the series. A cubic structure (space group $Pm\bar{3}m$) was also proposed for these compounds, but it was found that the data could be better fitted in a hexagonal structure (space group $R\bar{3}c$) as confirmed by the following neutron diffraction data refinement. It is difficult to use XRD patterns to determine the structural distortion, and the oxygen vacancy concentration. Accordingly, neutron diffraction was employed to distinguish the differences between the structures of the samples, and to determine the oxygen vacancy concentration.[38] Figure 2 shows the typical neutron patterns of the samples (N_2, O_2, and 50%CO/50%CO_2) at 290 K. The refinement parameters for all samples are listed in Table

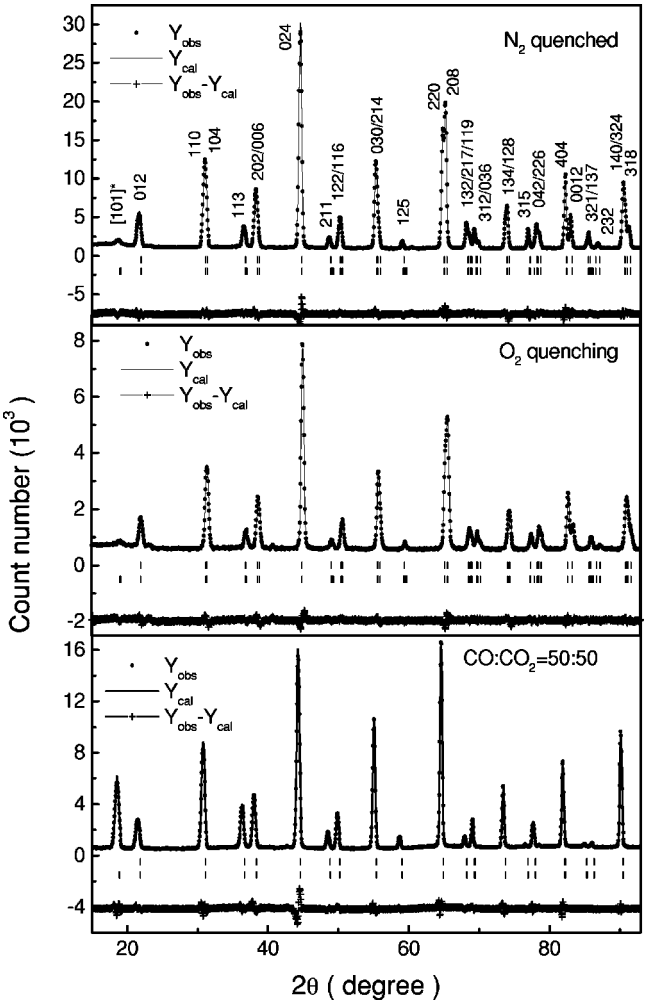

FIG. 2. Typical neutron diffraction patterns of $La_{0.6}Sr_{0.4}FeO_{3-\delta}$ quenched in N_2, O_2 and 50%CO:50%CO_2 at 290 K.(The bottom curves (Y_{obs}-Y_{cal}) are the difference between experimental data and refinement data. The vertical bars indicate the magnetic(bottom) and Bragg (top) peak positions).

II. The N_2-treated sample shows a rhombohedral structure and are refined in the space group $R\bar{3}c$. The diffraction peak half width for the CO/CO_2 treated samples is dramatically reduced compared to the N_2-treated samples which is similar to the XRD patterns. The rhombohedral splitting of the peaks is not too obvious for the CO/CO_2-treated samples. Thus, we have used both a cubic cell (space group $Pm\bar{3}m$) and a rhombohedral cell (space group $R\bar{3}c$) to refine the structure. The rhombohedral structure gives much better refinement results. For example, χ^2 is 7.56 for the refinement using space group $R\bar{3}c$ and 158 for space group $Pm\bar{3}m$ for the N_2-treated sample. Therefore, all samples have been refined with a rhombohedral cell (space group $R\bar{3}c$). The first diffraction peak ([101] at about 19°) is much stronger in the reduced samples than in the air-, N_2-, and O_2-quenched samples. This peak proves to be purely magnetic and the change reflects a large increase in magnetic moments for the CO/CO_2-reduced samples. The air-, O_2-, and N_2-quenched samples show similar patterns, and there is less than 1%

TABLE II. Refinement parameters of $La_{0.6}Sr_{0.4}FeO_{3-\delta}$ at 290 K. n is the occupation factor, x,y,z are the fractional position coordinates. m is the magnetic moment. V is the unit cell volume. B is the temperature factor. χ^2 is $[R_{wp}/R_{exp}]^2$, where R_{wp} is the residual error of the weighted profile and R_{exp} is statistically expected residual error of the entire measured scattering patterns.

x	A	B	C	D	E	F
a(Å)	5.5308(6)	5.5272(2)	5.5218(2)	5.53988(1)	5.5424(1)	5.5472(1)
c(Å)	13.4334(3)	13.4408(4)	13.4253(4)	13.5600(4)	13.5639(3)	13.5837(1)
V(Å^3)	355.88(7)	355.60(2)	354.50(3)	360.41(6)	360.84(7)	361.96(1)
La/Sr, 6a,z	0.25	0.25	0.25	0.25	0.25	0.25
Fe, 6b,x	0.167	0.167	0.167	0.167	0.167	0.167
O, 18e,x	0.5428(2)	0.5428(4)	0.5406(3)	0.5207(5)	0.5210(1)	0.5175(2)
n, La, 6a	0.1	0.1	0.1	0.1	0.1	0.1
n, Sr, 6a	0.067	0.067	0.067	0.067	0.067	0.067
n, O, 18e	0.500(3)	0.496(2)	0.496(2)	0.466(4)	0.459(4)	0.452(4)
B(Å), Fe, 6b	0.460(52)	0.743(38)	0.399(65)	1.082(49)	1.140(52)	1.248(58)
B(Å), O, 18e	0.689(104)	1.323(42)	0.875(71)	3.427(84)	3.184(85)	3.334(99)
B(Å), La(Sr), 6a	0.755(62)	0.932(45)	0.560(66)	1.446(63)	1.435(66)	1.845(78)
O vacancy (%)	0.0(6)	0.0(6)	0.0(4)	6.8(5)	8.1(5)	9.6(5)
m, Fe (μ_B)	1.17(15)	1.41(18)	1.13(10)	3.81(14)	3.83(15)	3.74(18)
χ^2 (%)	7.56	3.31	3.35	12.1	11.6	13.9

vacancies on the oxygen sites. The oxygen vacancy concentration is around 7–10% for the samples quenched in the CO/CO_2 mixtures. The unit cell volume of three CO/CO_2-reduced samples is larger by about 5 Å^3 than those of the air-, O_2- and N_2-quenched samples. The ratio of the lattice parameters a/c changes from 0.4112 for the air-quenched sample, to 0.40840 for the reduced samples which decreases the distortion from the cubic. This change affects the peak positions and the apparent sharpness of the diffraction peaks. An antiferromagnetic structure has been confirmed for all five samples. Fe atoms at (0,0,0) antiferromagnetically couple with those at (0,0,1/2) along the c axis. The Fe atom shows a magnetic moment of about $1.1–1.4\mu_B$ for N_2-, air-, and O_2-quenched samples at 290 K. A magnetic moment of $(3.7–3.8)\mu_B$ for the Fe atom is found for the CO/CO_2-quenched samples at 290 K. It is also evident that the magnetic space group $R\bar{3}c$ gives much better refinements than those of cubic cell, for examples, magnetic R factors of 8.0% and 31.1% are obtained for refinements with the $R\bar{3}c$ and $Pm\bar{3}m$ space groups, respectively. In Table III, we list the average bond length between the atoms and the Fe-O-Fe bond angle. It is found that the Fe-O and Fe-Fe bond lengths change less than 0.6%, while the bond angle of Fe-O-Fe linkage changes from 166° to 174°. The small change of the Fe-O and Fe-Fe bond length is due to the fact that there are oxygen vacancies that provide more relaxation space for Fe and O atoms. Since the Fe-Fe and the Fe-O distances do not show large change, the increase in the Fe-O-Fe bond angle increases the overlap between the Fe-O atomic orbitals and leads to a strong superexchange interaction between Fe-Fe. This enhanced superexchange interaction results in a high magnetic ordering temperature in the CO/CO_2-treated samples. The increase in the oxygen vacancy concentration changes the number of near neighbor oxygens with Fe, but this effect makes a smaller contribution to the superexchange interaction as compared to that of the bond angle change.

B. Magnetic properties

Figures 3 and 4 show the temperature dependence of the magnetization curves, under ZFC and FC using an applied

TABLE III. Magnetic ordering temperatures, average bond length between different atoms (bond length <4.0 Å), and Fe-O-Fe bond angle in $La_{0.6}Sr_{0.4}FeO_{3-\delta}$ quenched in different atmospheres.

	T_N/T_C (K)	Fe-O (Å)	Fe-O-Fe bond angle (deg)	La-O (Å)	Fe-Fe (Å)	O-O (Å)	La-La (Å)	La-Fe (Å)
A	315	1.972(1)	166.32	2.755(1)	2.789(3)	3.900(1)	3.900(1)	3.371(1)
B	325	1.964(2)	166.17	2.762(2)	2.777(4)	3.899(1)	3.899(2)	3.371(1)
C	325	1.960(3)	166.85	2.759(3)	2.772(3)	3.895(4)	3.895(2)	3.367(5)
D	790	1.961(4)	173.28	2.771(5)	2.774(4)	3.916(3)	3.916(3)	3.391(1)
E	800	1.962(4)	173.20	2.772(4)	2.775(5)	3.918(1)	3.918(1)	3.392(3)
F	>810	1.963(3)	174.35	2.774(1)	2.777(4)	3.922(1)	3.922(1)	3.396(2)

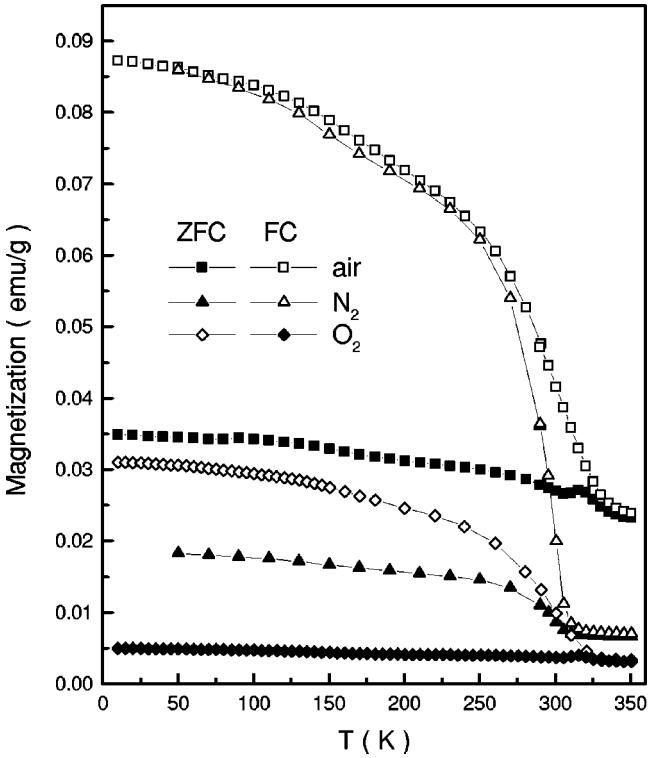

FIG. 3. The temperature dependence of the magnetization curves under field cooling (FC) and zero field cooling (ZFC) for $La_{0.6}Sr_{0.4}FeO_{3-\delta}$ quenched in N_2, air and O_2.

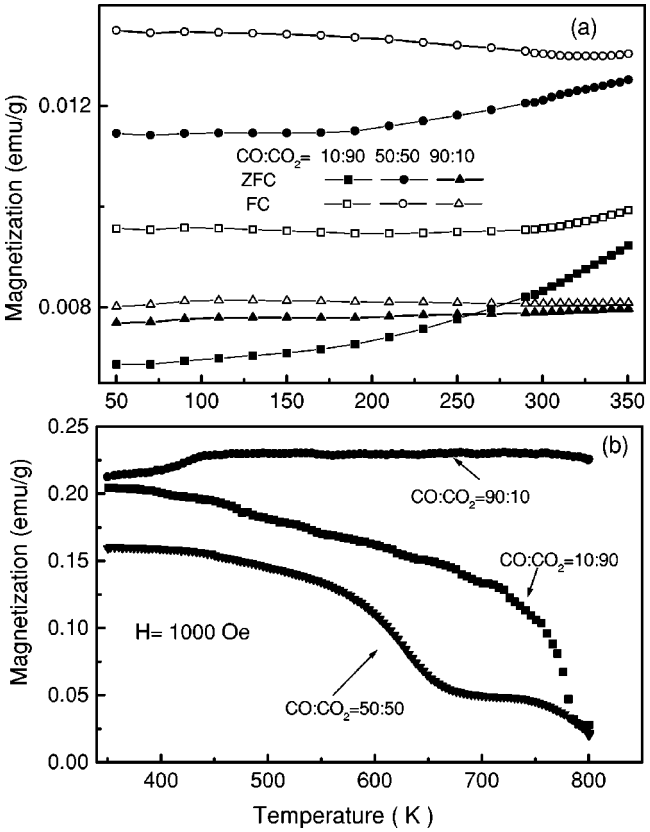

FIG. 4. (a) The temperature dependence of the magnetization curves under zero field cooling (solid symbols) and field cooling (open symbols) for $La_{0.6}Sr_{0.4}FeO_{3-\delta}$ quenched in $CO/CO_2=10:90$, $CO/CO_2=50:50$, $CO/CO_2=90:10$ mixtures; and (b) thermomagnetic curves from 350 to 800 K.

field of 50 Oe, for $La_{0.6}Sr_{0.4}FeO_{3-\delta}$ powders with varying heat treatment conditions. The difference between the FC and ZFC curves indicates the appearance of irreversibility for all compounds. The irreversibility might come from the alignments of the ferromagnetic component in the Fe sublattice. It is assumed that the external field also caused the spins to cant slightly out of their original direction.[39] This is in agreement with the results of the magnetic field dependence of the magnetization (Fig. 6). In particular for the N_2-, O_2-, and air-quenched samples, a large difference exists in the FC and ZFC curves below 300 K, suggesting a weak magnetic interaction between the spins. Due to the relatively larger contribution from the canted spins in the N_2-treated sample, the ZFC M-T curve of the N_2-treated sample shows a ferromagnetic characteristic, though the antiferromagnetic exchange coupling is predominant in this compound. The magnetic ordering temperatures T_C or T_N, 305, 325, and 325 K for the N_2-, O_2, and air-quenched samples, respectively, have been determined from the peak or the steep loss in the ZFC curves. The difference in the magnetization between the ZFC and FC curves decreases as the CO/CO_2 ratio increases from 10% to 90%. The Néel temperatures are far beyond 350 K for all CO/CO_2-quenched samples. Therefore the temperature dependence of magnetization from 350 to 800 K has been measured to determine the magnetic ordering temperature of CO/CO_2-quenched samples, as shown in Fig. 4(b). Magnetic ordering temperatures have been found to be higher than 800 K for all samples, which is higher than that for $LaFeO_3$ ($T_N=750$ K), and much higher than the normal $La_{0.6}Sr_{0.4}FeO_{3-\delta}$ compounds ($T_N=300$ K).[21] The increase of the magnetic ordering temperature is due to the increase of the superexchange interaction between the antiferromagnetic Fe ions. There are mainly three factors responsible for the change of the magnetic ordering temperatures. The first is the change in the Fe-O-Fe bond angle, the second is the Fe-O bond distance, and the third is the nearest number of neighbor ions. In the CO/CO_2-treated samples, the increase in the oxygen vacancy concentration leads to a small change in the Fe-O distances, but a large change in the Fe-O-Fe linkage angle. The increase of the Fe-O-Fe bond angle leads to a strengthening of the Fe-O-Fe exchange interaction which is manifested by a large increase in the Néel temperature. The increase in the oxygen vacancy concentration also changes the number of oxygen neighbors with Fe. However, as mentioned previously, this effect makes only a small contribution to the superexchange interaction, thus having little effect on the magnetic ordering temperatures. The small changes in the Fe-O bond length have small effect on the magnetic ordering temperatures. Similar phenomena have been observed in the $RFeO_3$ (R=rare earth) compounds, where the average Fe-O, and O-O distance are essentially constant for the entire rare earth series, although the dimensions of the unit cells decrease.[40] As R changes, only mutual positions of the oxygen octahedra change, and this leads to a change in the angle of the Fe-O-Fe valence bond, which affects the Néel temperature. It is noted that there is a kink in the magnetization

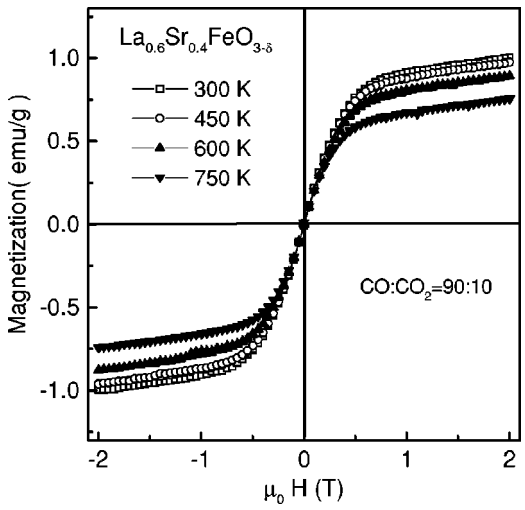

FIG. 5. Hysteresis loops of $La_{0.6}Mn_{0.4}FeO_{3-\delta}$ quenched in $CO/CO_2=90:10$ at different temperatures.

curve of the sample in Fig. 4(b), $CO:CO_2=50:50$ around 650 K, for which the reason is still not clear. It might be due to inhomogeneities in this sample.

Typical hysteresis loops of sample $CO:CO_2=90:10$ at different temperatures are displayed in Fig. 5. The coercivity and remanence are nearly zero at all temperatures. A ferromagnetic component is observed, and saturates at a magnetic field of $H=5$ kOe. The magnetization then linearly increases with the magnetic field due to the antiferromagnetic structure.

Figure 6 shows the magnetic field dependence of the magnetization for all samples at room temperature. The magnetization curves exhibit a strong dependence on the applied field. The magnetization can be described in terms of an Fe antiferromagnetic contribution and a weak ferromagnetic component.[41] The magnetization can be expressed as

$$\sigma=\sigma_0+\chi_a H, \tag{1}$$

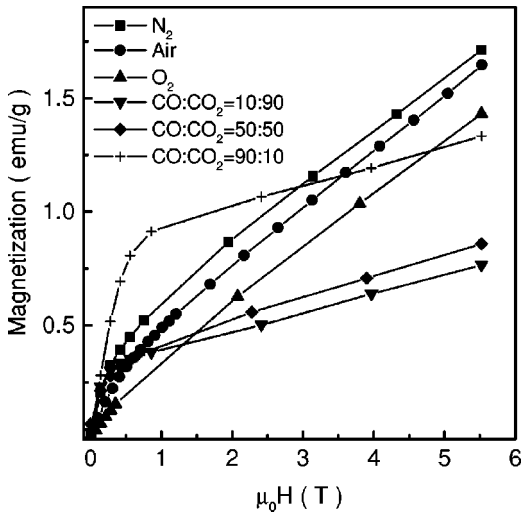

FIG. 6. Magnetization curves of $La_{0.6}Sr_{0.4}FeO_{3-\delta}$ quenched in N_2, air, O_2, and $CO/CO_2=10:90$, $CO/CO_2=50:50$, and $CO/CO_2=90:10$ at room temperature.

TABLE IV. Parameters σ_0 and χ_a for $La_{0.6}Sr_{0.4}FeO_{3-\delta}$ compounds at room temperature.

Samples	A	B	C	D	E	F
σ_0 (emu/g)	0.1907	0.0455	0.1629	0.2311	0.2261	0.4705
χ_a (emu/g T)	0.2910	0.2568	0.2772	0.1028	0.1222	0.1820

where χ_a is the antiferromagnetic susceptibility. The σ_0 is the ferromagnetic component (a constant). The corresponding σ_0 and χ_a are listed in Table IV. As can be seen, the ferromagnetic component σ_0 is smaller for N_2,- air- and O_2-quenched samples (A, B, and C) as compared to the CO/CO_2-quenched samples (D, E, and F). Results of the neutron diffraction refinements suggest that the parasitic ferromagnetism could be accounted for by a noncollinear molecular field which cants the two antiparallel sublattices due to the distortion of the crystal structure. The small canted angle between the moments of the Fe sublattice produces a small ferromagnetic moment.[42] The ferromagnetic component increases with increasing CO/CO_2 ratio, which may result in a high oxygen vacancy and increase the angle between the antiferromagnetically coupled sublattices. The susceptibilities of samples A, B, and C are larger than those of samples D, E, and F, which indicates that the latter are more difficult to magnetize. It is further evident that in the samples D, E, and F, a larger magnetic field is needed for saturation due to the strong superexchange interaction. This is in agreement with the higher magnetic ordering temperature in the CO/CO_2-treated samples. This is one possibility to explain the difference between the ZFC and FC curves for different samples. Since the CO/CO_2-treated samples show a larger anisotropy field, the field cooling will have less influence on the magnetization.

C. Mössbauer Studies

The ^{57}Fe Mössbauer spectra of $La_{0.6}Sr_{0.4}FeO_{3-\delta}$ are shown in Fig. 7. The Mössbauer spectra of N_2-, O_2-, and air-quenched samples show a paramagnetic or weak magnetic behavior because of the magnetic ordering temperature (300–325 K) being quite close to the room temperature. Two singlets were used in the fitting for the spectrum of the N_2-quenched sample. A relaxation of the hyperfine fields appears in the O_2- and air-quenched samples; therefore a Voigt peak-shaped sextet and a singlet were used in the fitting to account for the Fe^{3+} and Fe^{4+} ions.[21,22] The Mössbauer spectra of the CO/CO_2-quenched samples show a typical sextet due to the antiferromagnetic structure of the Fe atoms, which was confirmed by neutron diffraction and magnetic measurements. The best fitting can be reached by using two sextets for fitting the entire spectra by assuming two different Fe valence states. The hyperfine parameters are listed in Table V. The isomer shifts obtained for the N_2-, air-, and O_2-quenched samples are exactly what would be expected for valence states of Fe^{3+} and Fe^{4+} ions. The oxygen deficiency obtained from relative areas of the Mössbauer spectra of the Fe^{3+} and Fe^{4+} ions in the N_2-, air-, and O_2-treated samples is nearly zero, which agrees well with the neutron

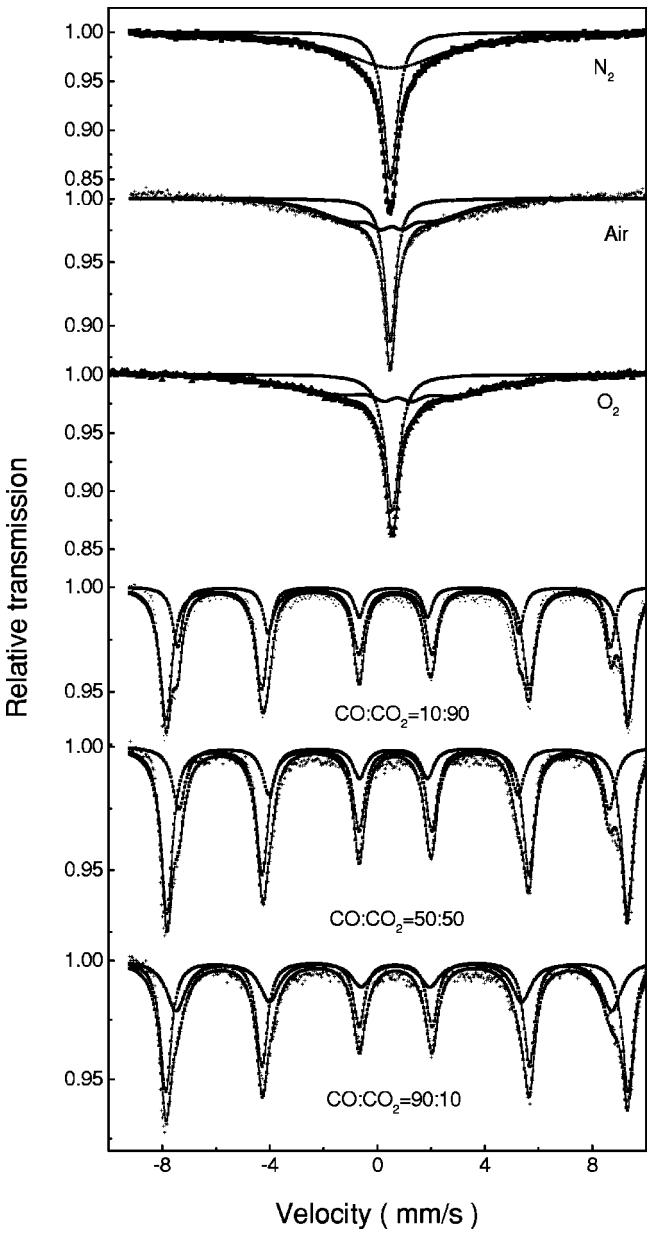

FIG. 7. Mössbauer spectra of $La_{0.6}Sr_{0.4}FeO_{3-\delta}$ quenched in different gases at room temperature.

diffraction measurements.[43,44] The spectra of CO/CO_2-quenched samples can be well fit with two magnetic sextets. The average hyperfine field is 53 T at room temperature, which is of the same order as that of the Fe oxide.[45] This large hyperfine field corresponds to the valence state between Fe^{2+} and Fe^{3+}. There is no evidence in the spectra for the presence of any Fe^{5+}, as has been noted in some studies.[21,22,28] An attempt to find evidence for the presence of distinct Fe^{4+} nor Fe^{2+} lines in the spectra also failed. The two sextets have values of the isomer shift somewhere between the Fe^{2+} and Fe^{3+} regions. The true oxidation state of Fe seems to be neither Fe^{2+} or Fe^{3+} but an intermediate state (such as $Fe^{3-\delta}$).[46] Because the CO/CO_2-treated samples have much higher oxygen vacancy concentrations as indicated by neutron data refinements, it suggests that some Fe^{4+} or even Fe^{3+} in the nonreduced samples are reduced to $Fe^{3-\delta}$ by the heat treatments in the CO/CO_2 mixture, in order to maintain charge balance in these compounds. According to the superexchange theory of Goodenough,[41] the superexchange interaction between $3d^5(Fe^{3+})$ and $3d^5(Fe^{3+})$ cations is antiferromagnetic, and is stronger than that between Fe^{4+} and Fe^{3+} ions, as well as that between Fe^{4+} and Fe^{4+} ions. Thus the decrease of the ratio of the Fe^{4+} ions as compared to the N_2-, O_2-, and air-quenched samples also increases the strength of the superexchange interaction between Fe ions, which results in a large hyperfine field, high Néel point, and a large magnetic moment. The average quadrupole splitting of the CO/CO_2-quenched samples is smaller than that of the nonreduced samples, which indicates a decrease in the distortion from the cubic structure. This is consistent with the neutron and x-ray diffraction data, which show a decrease of the distortion from cubic. It is found that the CO/CO_2-treated samples has the same a/c ratio (0.40855) as those ($a/c = 0.40850$) of $La_{1-x}Sr_xFeO_{3-\delta}$ ($x=0.6$ and 0.7), which is near the boundary between the rhombohedral and cubic structures.[22] This decrease in the a/c ratio of the reduced samples indicates a possible transformation from a rhombohedral to a pseudocubic structure by CO/CO_2 heat treatment.

IV. SUMMARY

Magnetic measurements, neutron diffraction, and Mössbauer spectroscopy have been used to study the structure and

TABLE V. Hyperfine filed (B_{hf}), isomer shift (IS), quadrupolar splitting (QS), and relative intensity (Int.) of $La_{0.6}Sr_{0.4}FeO_{3-\delta}$ quenched at different gases at room temperature.

	Fe^{3+}				Fe^{4+}			
	B_{hf} (T)	IS (mm/s)	QS (mm/s)	Int. (%)	B_{hf} (T)	IS (mm/s)	QS (mm/s)	Int. (%)
A		0.261(2)		63.9		0.180(4)		36.1
B	15.2(4)	0.263(2)	0.058(3)	59.7		0.170(3)		40.3
C	19.1(3)	0.331(3)	0.047(3)	59.9		0.202(4)		40.1
		I				II		
D	53.5(2)	0.324(4)	0.050(1)	73.0	50.1	0.236(4)	0.020(3)	27.0
E	53.3(2)	0.325(3)	0.056(3)	70.1	49.8	0.236(4)	0.021(5)	29.1
F	53.5(3)	0.324(3)	0.035(4)	59.7	50.4	0.272(3)	−0.063(2)	40.3

physical properties of $La_{0.6}Sr_{0.4}FeO_{3-\delta}$ prepared by varying heat treatments in different environments. All materials are single phase and crystallize in the rhombohedral perovskite structure, space group $R\bar{3}c$. CO/CO_2-heat-treated samples show large amounts of oxygen vacancies, which decrease the distortion from a cubic structure. The oxygen vacancy concentration increases from 6.8% to 9.6% as the ratio of CO/CO_2 changes from 10% to 90%. A magnetic moment of $3.8\mu_B$ and a hyperfine field of 53 T have been observed for Fe atoms in the CO/CO_2-quenched samples, whereas in the O_2- and air-quenched samples, the Fe atoms have a magnetic moment of $(1.2-1.4)\mu_B$ and a hyperfine field of 15–18 T. The heat treatment in the CO/CO_2 atmosphere creates oxygen vacancies and increases the unit cell volume. However, it maintains the Fe-Fe and Fe-O distances nearly constant, thus changing the *x* coordinate of the oxygen octhedra, leading to a larger Fe-O-Fe bond angle, which thus enhances the superexchange interaction between the Fe-Fe ions. The change of the Fe-O-Fe bond angle and the change in the valence states of the Fe ions in the CO/CO_2-treated samples play a key role in the increase of the Néel temperature, the magnetic moments, and the hyperfine fields. It is interesting to note that the exchange interaction in this pervoskitic structure is controlled by the *x* coordinate of oxygen, which changes the Fe-O-Fe bond angle, while maintaining the rhombohedral structure.

ACKNOWLEDGMENTS

The financial support of the National Science Foundation through Grant No. DMR-9614596, the Defense Advanced Research Projects Agency through Grant No. DAAG 55-98-1-0267, and the support by DOE under DOE Contract No. DE-FC26-99FT400054 and UFA99-0038 are acknowledged. The authors thank Dr. J. Diederichs of Quantum Design for their help with the SQUID measurements.

[1] M. B. Salamon and M. Jaime, Rev. Mod. Phys. **73**, 583 (2001).
[2] Y. Tokura, *Contribution to Colossal Magnetoresistance Oxides*, edited by Y. Tokura (Gordon & Breach, London, 1999).
[3] M. Imada, A. Fujimori, and Y. Tokura, Rev. Mod. Phys. **70**, 1039 (1998).
[4] A. P. Ramirez, J. Phys.: Condens. Matter **9**, 8171 (1997).
[5] *Colossal Magnetoresistance, Charge Ordering and Related Properties of Manganese Oxides*, edited by C. N. R. Rao and B. Raveau (World Scientific, Singapore, 1998).
[6] J. M. D. Coey, M. Viret, and S. von Molnar, Adv. Phys. **48**, 167 (1999).
[7] *Physics of Manganites*, edited by T. Kaplan and S. Mahanty (Kluwer Academic/Plenum, New York, 1999).
[8] V. M. Loktev and Yu.G. Pogorelov, Fiz. Nizk. Temp. **26**, 231 (2000) [Low Temp. Phys. **26**, 171 (2000)].
[9] J. M. Ralph, J. T. Vaughey, and M. Krumpelt, in *Solid Oxide Fuel Cells VII*, Proceedings of the Seventh International Symposium, edited by H. Yokokawa and S.C. Singhal (Electrochemical Society, Pennington, New Jersey, 2001), pp. 466–475.
[10] V. V. Kharton, A. P. Viskup, E. N. Naumovich, and V. N. Tikhonovich, Mater. Res. Bull. **34**, 1311 (1999).
[11] C. C. Chen, M. M. Nasrallah, H. U. Anderson, and M. A. Alim, J. Electrochem. Soc. **142**, 491 (1995).
[12] K. Huang, J. Wang, and J. B. Goodenough, J. Mater. Sci. **36**, 1093 (2001).
[13] J. B. Goodenough, in *Progress in Solid State Chemistry*, edited by H. Reiss (Pergamon, London, 1971) Vol. 5, p. 145.
[14] J. B. MacChesney, R. C. Sherwood, and J. F. Potter, J. Chem. Phys. **43**, 1907 (1965).
[15] P. K. Gallagher, J. B. MacChesney, and D. N. E. Buchanan, J. Chem. Phys. **41**, 2429 (1964).
[16] M. Takano, N. Nakanishi, Y. Takeda, S. Naka, and T. Takada, Mater. Res. Bull. **12**, 923 (1977).
[17] P. M. Woodward, D. E. Cox, E. Moshopoulou, A. W. Sleight, and S. Morimoto, Phys. Rev. B **62**, 844 (2000).
[18] J. P. Hodges, S. Short, J. D. Jorgensen, X. Xiong, B. Dabrowski, S. M. Mini, and C. W. Kimball, J. Solid State Chem. **151**, 190 (2000).
[19] A. E. Bocquet, A. Fujimori, T. Mizokawa, T. Saitoh, H. Namatame, S. Suga, N. Kimizuka, Y. Takeda, and M. Takano, Phys. Rev. B **45**, 1561 (1992).
[20] M. Takano, J. Kawachi, N. Nakanishi, and Y. Takeda, J. Solid State Chem. **39**, 75 (1981).
[21] U. Shimony and J. M. Knudsen, Phys. Rev. B **144**, 361 (1966).
[22] S. E. Dann, D. B. Currie, M. T. Weller, M. F. Thomas, and A. D. Al-Rawwas, J. Solid State Chem. **109**, 134 (1994).
[23] A.D. Al-Rawwas, C. E. Johnson, M. F. Thomas, and S. E. Dann, and M. T. Weller, Hyperfine Interact. **93**, 1521 (1994).
[24] G. H. Jonker and J. H. van Santen, Physica (Amsterdam) **19**, 120 (1953); G. H. Jonker and J. H. Van Santen, *ibid.* **16**, 599 (1950).
[25] P. M. Raccah and J. B. Goodenough, J. Appl. Phys. **39**, 1209 (1968).
[26] V. G. Bhide, D. S. Rajoria, C. N. R. Rao, G. Rama Rao, and V. G. Jadhao, Phys. Rev. B **12**, 2832 (1975).
[27] J. Grenier, N. Ea, M. Pouchard, and M. M. Abou-Sekkina, Mater. Res. Bull. **19**, 1301 (1984).
[28] P. D. Battle, T. C. Gibb, and S. Nixon, J. Solid State Chem. **77**, 124 (1988).
[29] J. Q. Li, Y. Matsui, S. K. Park, and Y. Tokura, Phys. Rev. Lett. **79**, 297 (1997).
[30] Y. R. Uhm, S. W. Lee, K. T. Park, Y. Tomioka, Y. Tokura, and C. S. Kim, J. Appl. Phys. **87**, 4873 (2000).
[31] R. Kajimoto, Y. Oohara, M. Kubota, H. Yoshizawa, S. K. Park, Y. Taguchi, and Y. Tokura, J. Phys. Chem. Solids **62**, 321 (2001).
[32] B. C. Hauback, H. Fjellvag, and N. Saito, J. Solid State Chem. **124**, 43 (1996).
[33] C. Ritter, M. R. Ibarra, J. M. DeTeresa, P. A. Algarabel, C. Marquina, J. Blasco, J. Garcia, S. Oseroff, and S. W. Cheong, Phys. Rev. B **56**, 8902 (1997).
[34] J. A. M. Van Roosmalen and E. H. P. Cordfunke, J. Solid State Chem. **110**, 106 (1994); **110**, 109 (1994); **110**, 113 (1994); **93**, 212 (1991).

[35] M. P. Pechini, U.S. Patent No. 3,330,697, July 1967.
[36] N. G. Eror and H. U. Anderson, in *Better Ceramics through Chemistry II*, edited by C. J. Brinker, D. E. Clark, and D. R. Ulrich (Materials Research Society, 1986), pp. 571–577.
[37] J. Rodriguez-Carvajal, FULLPROF program, Version 3.d (1998).
[38] D. E. Cox, IEEE Trans. Magn. **MAG-8**, 161 (1972).
[39] V. P. S. Awana, S. X. Dou, I. Felner, I. Nowik, S. K. Malik, A. Metha, R. Singh, A. V. Narlikar, and W. B. Yelon, J. Appl. Phys. **83**, 7312 (1998).
[40] M. Marezio, J. P. Remeika, and P. D. Dernier, Acta Crystallogr., Sect. B: Struct. Crystallogr. Cryst. Chem. **26**, 2008 (1970).
[41] J. B. Goodenough, in *Magnetism and Chemical Bond*, edited by F. Albert Cotton (Interscience, London, 1963), Vol. 1, p. 154.
[42] V. E. Naish and E. A. Turov, Fiz. Met. Metalloved. **11**, 161 (1961); **11**, 321 (1961); **9**, 10 (1960).
[43] G. J. Long, D. Hautot, A. Mohn, I. Kaus, and H. U. Anderson, J. Appl. Phys. **85**, 7312 (1999).
[44] P. D. Battle, T. C. Gibb, and S. Nixon, J. Solid State Chem. **79**, 75 (1988).
[45] R. Bauminger, S. G. Cohen, A. Marinov, S. Ofer, and E. Segal, Phys. Rev. **122**, 1447 (1961).
[46] Y. M. Zhao, R. Mahendiran, N. Nguyen, B. Raveau, and R. H. Yao, Phys. Rev. B **64**, 024414 (2001).